# Journal of Materials Chemistry C

Check for updates

# Controlling the device functionality by solvent engineering, solar cell *versus* light emitting diode†

Shir Yudco, [ID] Adva Shpatz Dayan, Bat-El Cohen, Tal Binyamin and Lioz Etgar [ID] *

In this work we studied inverted perovskite device structure which can function as a solar cell and as a light emitting diode (LED) simultaneously. We found that changing the solvent ratio, Dimethyl sulfoxide (DMSO) to Dimethyl formamide (DMF) in the perovskite solution has a dramatic effect on the device functionality. It was observed that the solvent ratio significantly affects the perovskite layer leading to opposite optimization functionality. In the case of only DMF the devices function efficiently as an LED with a preferability for radiative recombination as was measured by photoluminescence lifetime and electroluminescence (EL) demonstrating external quantum efficiency (EQE) of 10.8%. When adding DMSO to the perovskite solution the device showed an increase in the efficiency as a solar cell and a reduction in its EL with a power conversion efficiency of 14.4%. This is mainly due to adjustment in the thickness and uniformity of the perovskite layer with less $PbI_2$ residues (as a result of the addition of the DMSO) measured by X-ray diffraction. This work demonstrates the ability to control the device functionality between solar cell and LED by the solvent ratio in the perovskite's precursor solution.

## Introduction

Hybrid organic–inorganic perovskite has proven in recent years to be a promising photovoltaic (PV) material for both solar cells[1–3] and LED[4,5] devices. Advantages such as high absorption coefficients, tunable band gap and low cost materials make perovskite solar cells a highly studied field achieving efficiency which exceed 25%.[6–8] Perovskite properties such as high photoluminescence quantum yield (PLQY) and efficient electroluminescence (EL) paved the way to the development of perovskite light emitting diode (PeLED),[9,10] which can currently reach external quantum efficiency (EQE) of over 20%[11–14] with green, red and Near IR emission wavelength. Since the perovskite can have a band gap in the Near IR region it is very attractive for both solar cells and LED devices. Near IR bandgap increases the absorption spectra of the solar cell while opening the possibility to manufacture Near IR PeLED which can be used in a variety of technologies such as optic fibers, imaging and IR sensors.

The way to improve perovskite based devices requires optimization of the perovskite layer and the device architecture. Investigation of all the parameters is needed for the device optimization, including perovskite and solvent composition, deposition methods, interface engineering and compatibility of the hole and electron transport layers (HTL and ETL). The

most standard perovskite composition for efficient PV cells is $MAPbI_3$,[1] where compositional changes of the cation and halide positions to a mix halide mix cation perovskite generated a wider band gap and good thermal stability.[15,16] Another important aspect in improving the perovskite layer, for both solar cells and LED, is solvent composition of the perovskite solution. There is a direct connection between the perovskite solvents and the resulting film quality.[17,18] To-date there are two main ways to deposit the perovskite, two step and one step deposition which require different conditions.[19,20] Choosing the right device architecture is important for interface engineering, which is strongly depended on the compatibility between the perovskite, HTL and ETL layers. The most common device architectures are mesoscopic n–i–p,[21] planar n–i–p[22] and inverted p–i–n.[23] The inverted structure open the way to low temperature fabrication and minimize the hysteresis.[24,25] Here we used a mix halide mix cation perovskite, using one step deposition method and inverted p–i–n structure, while focusing on the influence of the solvent composition.

Recent development in perovskite based devices presented the possibility of a dual functionality as a solar cell and as an LED.[26,27] Studying the performance of the perovskite as a light harvester and as a light emitter material in the same device sheds light on the perovskite's functionality. Using a combination of LED and PV performance can predict the perovskite's layer properties, and can improve the understanding of nonradiative recombination inside perovskite based devices.[28–31] Moreover this dual functionality can be used to study the parameters influencing the performance, in order to optimize them both as a solar cell and as an LED.

*Institute of Chemistry, Casali Center for Applied Chemistry and the Center for Nanoscience and Nanotechnology, The Hebrew University of Jerusalem, Jerusalem 91904, Israel. E-mail: lioz.etgar@mail.huji.ac.il*
† Electronic supplementary information (ESI) available. See DOI: **https://doi.org/10.1039/d2tc01941h**

In this work we used a mixture of two solvents-dimethyl formamide (DMF) and Dimethyl sulfoxide (DMSO), where DMSO has a double purpose as a co-solvent and as a tool to control the perovskite crystallization.[32,33] A $PbI_2$–DMSO complex is formed inside the precursors solution. DMSO is a Lewis base with a lone pair of electrons on the oxygen, that react with the $Pb^{2+}$ in the $PbI_2$ Lewis acid, thus creating a complex of $PbI_2$–DMSO.[34,35] This complex can be formed with other solvents such as DMF, but the DMSO is more polar then the DMF and therefore creates a more stable bond with $PbI_2$. The polarity differences between the solvents has an additional effect on the compatibility between the perovskite solution and the layer beneath it,[36] by optimizing the perovskite solvents to the substrate a more uniform layer with less pinholes can be formed.

We study the influence of the perovskite's solvent composition on the perovskite layer functionality as a light emitter and as a light harvester in LED and solar cell respectively. The solvent ratio was varied from a DMSO : DMF ratio of 0.2 : 0.8 to 0.0 : 1.0 (*i.e.* without DMSO). We tracked the film formation of the perovskite for different DMSO : DMF ratios and implemented them in complete devices which can function simultaneously as an LED and as a solar cell. It was observed that the solvent ratio can control the device functionality between LED and solar cell.

## Results and discussion

Mix halide mix cation perovskite was synthesized,[37,38] with the chemical formula $(FA_{0.8}Cs_{0.2})Pb(I_{0.87}Br_{0.13})_3$, while the perovskite

functioned as light harvester and as light emitter in the same device architecture, *i.e.* as a solar cell and as an LED.

It was reported that adding DMSO to the perovskite precursor solution can enhance the PV performance of the perovskite based solar cells.[39–41] In this work we studied how the solvent ratio DMSO/DMF affects the performance of the device, when it is being used as a solar cell and as an LED.

Cross section SEM images of cells with different DMSO : DMF ratio are presented in Fig. 1a and Fig. S1a–d (ESI†). The SEM measurements showed a significant change in the perovskite layer thickness as a result of the addition of DMSO. Perovskite films synthesized without DMSO (using only DMF) showed an average layer thickness of 870 nm ± 70 nm, and formed a non-uniform layer without clear grain boundaries and high concentration of pin holes. When adding more DMSO to the perovskite precursor solution the perovskite layer is more uniform and thinner. Perovskite films with DMSO : DMF ratios of 0.05 : 0.95 and 0.1 : 0.9 showed an average layer thickness of 740 nm ± 10 nm and 680 ± 50 nm respectively. While perovskite films with DMSO : DMF ratio of 0.2 : 0.8 presented an average layer thickness of 460 nm ± 30 nm and showed better layer uniformity than the case without DMSO. A summary of the layer thickness as a function of the solvent ratio can be found in Fig. 1b.

The thickness of the perovskite layer is important in order to achieve the optimal light absorbance. Based on the perovskite's absorption coefficient the optimal layer thickness for perovskite solar cells is *ca.* 400 nm[42] and depends on the perovskite composition and the grain size. The perovskite composition
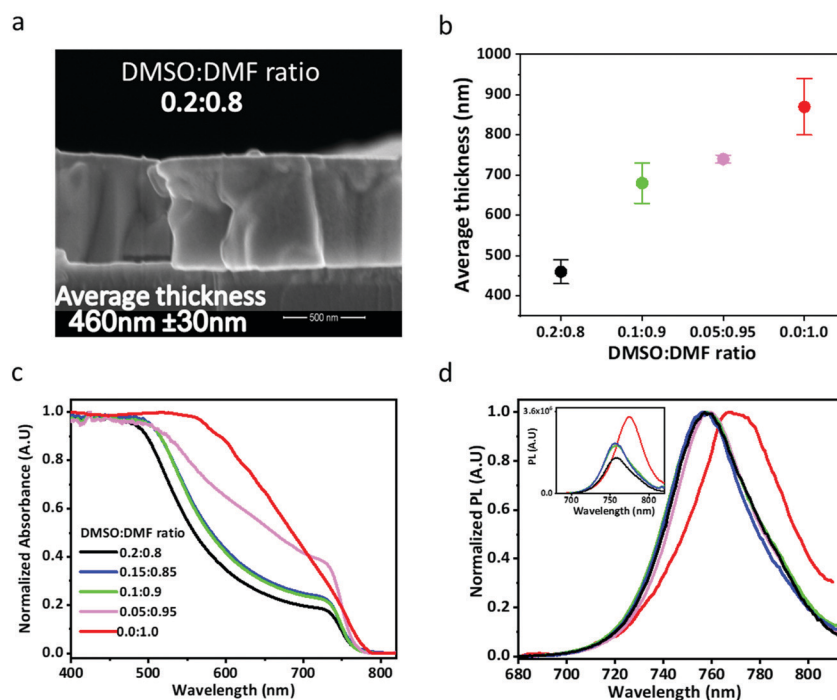


Fig. 1 (a) Cross section SEM image of device with 0.2 : 0.8 DMSO : DMF ratio, with an average perovskite layer thickness of 460 nm. (b) Perovskite layer thickness as a function of DMSO : DMF ratio. (c) Absorbance for all DMSO : DMF ratios. (d) Normalized photoluminescence and un-normalized Photoluminescence (inset).
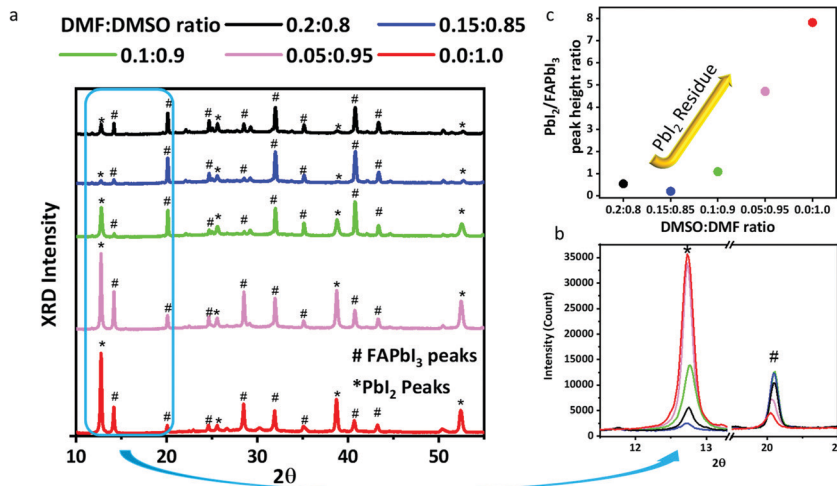
**Fig. 2** (a) XRD measurements for all DMSO : DMF ratios. (b) Enlargement of the XRD spectra for all DMSO : DMF ratios for 12.7° (PbI$_2$ peak) and 20° (FAPbI$_3$ peak). (c) PbI$_2$/FAPbI$_3$ peak height ratio, representing PbI$_2$ residue in the perovskite layer as a function of DMSO : DMF ratio.

was kept constant for all solvent ratios, as was verified by the XRD analysis in Fig. 2. The grain size did not change significantly by the change in the solvent ratio, Table S1 (ESI†) summarizes the average grain size as was measured from top view SEM, an average of $130 \pm 27$ nm was measured for 0.2 : 0.8, 0.15 : 0.85 and 0.1 : 0.9 DMSO : DMF ratios, at 0.05 : 0.95 and 0.0 : 1.0 the average size slightly decreased to $123 \pm 20$ nm and $105 \pm 27$ nm respectively. This decrease is negligible in comparison to the increase in the layer thickness. Controlling the perovskite layer thickness and grain size can also be done by changing the precursor solution concentration, often leading to an improvement in the solar cells performance.[25,43] Contrary to that, reducing the grain size can improve the EQE of the PeLEDs.[44,45] Our results show that changing the solvent ratio influence the layer thickness and the layer uniformity significantly, yet had only a minor effect on the grain size. Therefore, the change in the perovskite layer thickness affects the light absorbance and as a result the performance of the device. In the case of a perovskite layer thickness over 800 nm (only DMF) the light absorption is not optimal and there are pathways for radiative and non-radiative recombination, which influence the device performance mainly as a solar cell.

The change in the absorbance of the perovskite at various solvent ratios can be seen in Fig. 1c. While the absorbance of 0.2 till 0.05 DMSO ratios has the same shape, in the case of perovskite with only DMF (0.0 DMSO ratio) the absorbance shape shows a gradually increment until it reaches to saturation which suggest on a thick perovskite layer. Interestingly even when adding a small amount of DMSO to the DMF based perovskite solution the absorbance shape is greatly affected.

Fig. 1d shows the normalized PL spectra of the studied DMSO : DMF ratios. In the case of 0.0 : 1.0 DMSO : DMF films (only DMF) a red shift in the PL is observed. This shift may be related to emission from sub band gap levels. As can be seen in the SEM cross section (Fig. S1d, ESI†) and top view SEM (Fig. S2c, ESI†) the perovskite layer (in the case of DMF only)

has lower uniformity and more pin holes. This can result with traps and sub band gap levels which can explain the red shift of the PL.[46] The PL lifetime can be found in Fig. S3 (ESI†), the longest life time was observed in the case of only DMF film while the life time is getting shorter when adding more DMSO to the perovskite solution (Table S2, ESI†). The longer life time indicates on high radiative recombination in the perovskite's grains which might be favorable in the case of electroluminescence (EL) intensity (discussed in details below). On the other hand, the addition of DMSO decreased the life time which suggest on more channels for non-radiative recombination.[47]

The change in the layer uniformity of the perovskite due to the DMSO : DMF solvent ratio can be explained by the properties of the different solvents. Both DMF and DMSO are polar aprotic solvents, yet the DMSO has a higher dipole moment which creates a stronger coordinative bond with the PbI$_2$ then the DMF, leading to a DMSO–PbI$_2$ complex in the perovskite solution.[18,48] This complex is vital for the formation of a uniform layer, as is clearly evident from the cross-section SEM images. While in Fig. 1a for a higher DMSO ratio a uniform layer was formed, in Fig. S1(c and d) (ESI†) for low DMSO ratio and no DMSO a non-uniform layer with pinholes can be seen. The addition of DMSO slows the perovskite crystallization due to higher boiling point (189 °C *vs.* 153 °C) and viscosity with lower vapor pressure (1.10 g mL$^{-1}$ *vs.* 0.944 g mL$^{-1}$) compared to DMF.[17,49] In the case of DMF it starts to evaporate during the spin coating process while the DMSO stays bond to the PbI$_2$ and evaporates during the annealing step following the spin coating. Therefore the addition of DMSO enables a slower crystallization leading to the formation of a more uniform perovskite layer as can be seen in the case of 0.2 : 0.8 DMSO : DMF ratio in Fig. 1a.

Recently hall effect measurements were successfully used to characterize perovskite solar cells.[50–52] Table S3 (ESI†) presents the results of the hall effect measurements that were performed in this work. The measurements were done on two DMSO : DMF

ratios with the most and the least amount of DMSO (0.2 : 0.8, 0.0 : 1.0). The change in the solvent ratio did not change the hall mobility in the perovskite layer, $7.19 \times 10^{-1}$ cm$^2$ V$^{-1}$ s$^{-1}$ and $8.67 \times 10^{-1}$ cm$^2$ V$^{-1}$ s$^{-1}$ were measured for 0.0 : 0.1 and 0.2 : 0.8 DMSO : DMF ratios respectively. However, the carrier concentration for 0.2 : 0.8 is higher than for 0.0 : 0.1, correspond to $2.81 \times 10^{+15}$ cm$^{-3}$ and $4.97 \times 10^{+14}$ cm$^{-3}$ respectively. This can support the better functionality of the 0.2 : 0.8 ratio in the solar cell (as discussed below).

Fig. 2 presents XRD measurement of the different DMSO : DMF ratios. In all cases the same peaks were found, which suggests that the solvent ratio doesn't influence the formation of different perovskite phases. The XRD peaks are matched with two known materials compositions-FAPbI$_3$ and PbI$_2$ diffraction peaks. Full width half maximum (FWHM) of the FAPbI$_3$ peak show high crystallinity when DMSO is added, observing a change in the FWHM from 0.19 to 0.14 for perovskite solution without DMSO and 0.2 : 0.8 DMSO : DMF ratio respectively. Improved crystallinity at high DMSO ratios matches the improved layer uniformity previously discussed from the SEM images (Fig. S1, ESI†). Fig. 2b shows the enlargement of the main peaks of PbI$_2$ at 12.7 degree and FAPbI$_3$ at 20 degree for the various DMSO : DMF ratios. As can be seen there is a change in both peak's intensities as a function of the DMSO : DMF ratio. As the amount of DMSO is decreasing the intensity of the PbI$_2$ peak is increased in comparison to the FAPbI$_3$ peak. The ratio of the peak intensity for PbI$_2$/FAPbI$_3$ is shown in Fig. 2c. The amount of PbI$_2$ residues is increasing when lower amount of DMSO is being used. It can be concluded that without DMSO the conversion of the precursors into perovskite is less favorable in comparison to the addition of DMSO to the perovskite solution. There is more

PbI$_2$ residues in the perovskite film when DMSO is not used.[53] As was previously mentioned the DMSO is forming a complex with the PbI$_2$, which slows down the evaporation of the solvent and support the lower amount of PbI$_2$ which left in the perovskite film.

Complete devices of the inverted architecture[54,55] (Fig. 3a) were fabricated on a conductive Indium Tin Oxide (ITO) substrate, with MeO–2PACz ([2-(3,6-dimethoxy-9H-carbazol-9-yl)ethyl]-phosphonic acid) as HTL, MeO–2PACz creates a self-assembled monolayer (SAM) on the ITO surface.[56] [6,6]-Phenyl-C61-butyric acid methyl ester (PCBM) and 2,9-dimethyl-4,7-diphenyl-1,10-phenanthroline (BCP) were used as ETL, on top of the ETL Ag electrode was thermally evaporated. First we studied how these devices function as a solar cell when the perovskite layer was synthesized using different solvent ratios (DMSO : DMF). Other parameters in the device were held constant in order to study the effect of the solvents in the perovskite precursors solution on the PV performance and the LED performance. A clear trend in the power conversion efficiency (PCE) vs. the solvent ratio was observed, as the DMSO ratio is increasing the PCE increased (Fig. 3b). In the case of only DMF the average PCE is the lowest reaching 3%, where at 0.2 : 0.8 DMSO : DMF ratio the PCE improves to an average of 13.5% (a summary of the average PV parameters for all DMSO : DMF ratios can be found in Table S4, ESI†). 0.2 : 0.8 DMSO : DMF ratio was found to be the optimal solvent ratio for the solar cell, when increasing the DMSO above this ratio the PCE starts to decrease as can be seen in Fig. S6a (ESI†).

Fig. 3c and d show the FF and the $J_{sc}$ of each solvent ratio. Both the FF and the $J_{sc}$ decrease as the DMSO ratio is decreasing. The $J_{sc}$ shows a similar trend to the PCE with a linear decrease in correlation to the DMSO ratio, while the FF has a
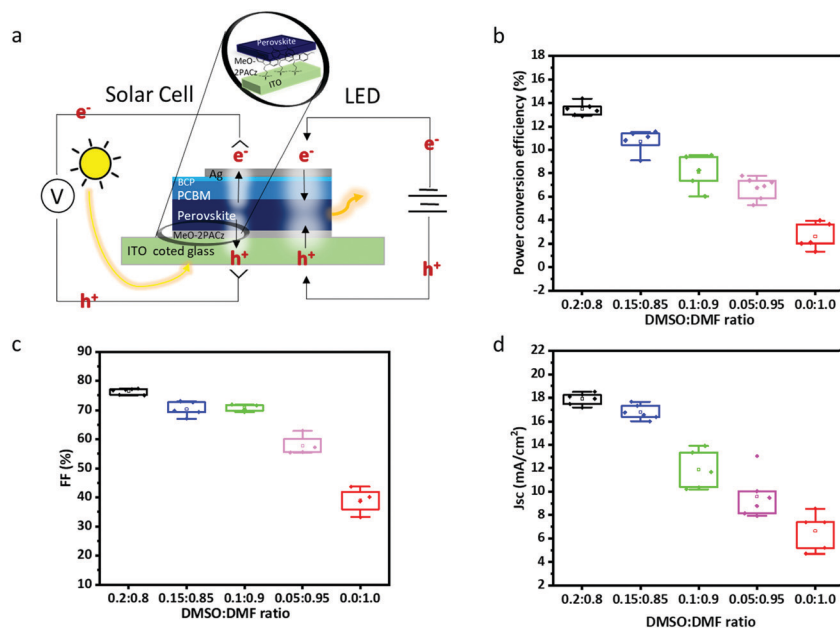


**Fig. 3** PV parameters of perovskite solar cells at different DMSO : DMF ratios. (a) Schematic structure of the perovskite dual functionality device fabricated in this work; (b) power conversion efficiency (PCE); (c) fill factor (FF) and (d) short circuit current density ($J_{sc}$).

moderate decline. $J_{sc}$ indicates a better charge transfer in the device, which support a reduction in the charge recombination, agree well with the decrease in the EQE and EL intensity when increasing the DMSO ratio (Fig. 4a and b respectively). It is suggested that even small amount of DMSO in the perovskite film reduces the radiative recombination. The moderate decline in the FF can be explained by the $V_{oc}$ as a function of the solvent ratio (Fig. S4b, ESI†). The average $V_{oc}$ of all the solvent ratios did not change significantly or consistently (as can also be seen in the $JV$ curves in Fig. S4a, ESI†), which agree with the moderate change of the FF.

The change in the $J_{sc}$ and FF can also be related to traps inside the band gap, as was seen by longer PL lifetime and red shift in the PL (Fig. S3 (ESI†) and Fig. 1d). These traps can lead to quenching of the photocurrent inside the solar cell. The changes in the PV performance can also be explained by the increase in the perovskite thickness as was observed from the SEM images (Fig. 1a, b and Fig. S1a–d, ESI†). While cells with solvent ratio of 0.2 : 0.8 DMSO : DMF achieved a maximum PCE of 14.4% with an average layer thickness of 460 nm ± 30 nm. Solar cells prepared with only DMF achieved a maximum PCE of 3.9%, with an average layer thickness of 870 nm ± 70 nm. The light penetration depth of perovskite is estimated to be 660 nm,[57] depending on the absorption coefficient and wavelength, therefore at layer thickness of over 800 nm (only DMF) the light absorption is not optimal, which result with significantly lower solar cell performance compared to the case of 0.2 : 0.8 DMSO : DMF ratio. Moreover, in the case of thick perovskite layer there are more options for radiative and non-radiative pathways for charge recombination loss which affects the FF (the average FF of 0.2 : 0.8 DMSO : DMF ratio is 76% while the average FF without DMSO is 42%) and reduce the PCE of the solar cells.

Following the analysis of the device as a solar cell we study its functionality as an LED. An opposite trend of the LED performance as a function of the solvent ratio was observed. Fig. 4a–c show improvements in the LED performance as the DMSO amount is reduced. The EL measurements (Fig. 4a) were performed by scanning the voltage while measuring the EL intensity and EL peak position. The EL intensity is stronger by 2 orders of magnitude in devices with only DMF (0.0 : 1.0 ratio) than in the case of 0.2 : 0.8 DMSO : DMF ratio, reaching a maximum intensity of 1.1 watt m$^{-2}$ and 0.05 watt m$^{-2}$ respectively. Fig. 4b shows the same improvement in the External Quantum Efficiency (EQE) of the LED, starting from 0.3% for 0.2 : 0.8 DMSO : DMF ratio and increasing to EQE of 10.8%. (When increasing further the DMSO the EQE is not changing anymore, Fig. S6b, ESI†) Another improvement can be seen in the current efficiency (CE, Fig. 4c) which increased significantly from 0.005 cd A$^{-1}$ at 0.2 : 0.8 DMSO : DMF to 0.27 cd A$^{-1}$ for only DMF. The relatively low CE can be related to leakage currents (the currents can be seen in the $JV$ curves in Fig. S5c, ESI†), while the improvement in the CE is related to the increase in the EL intensity (EL intensity for all solvent ratios in cd m$^{-2}$ can be found in Fig. S5a, ESI†). Fig. 4e presents three-dimensional graph of the EL intensity as a function of the applied voltage and the EL peak position.

The increase in the EL intensity can be attributed to the improvement in the radiative recombination in the perovskite film, as was also observed from the PL intensity and the PL lifetime measurements (Fig. 1d and Fig. S3, ESI†). In addition, based on the XRD measurements (Fig. 2) it was observed that in
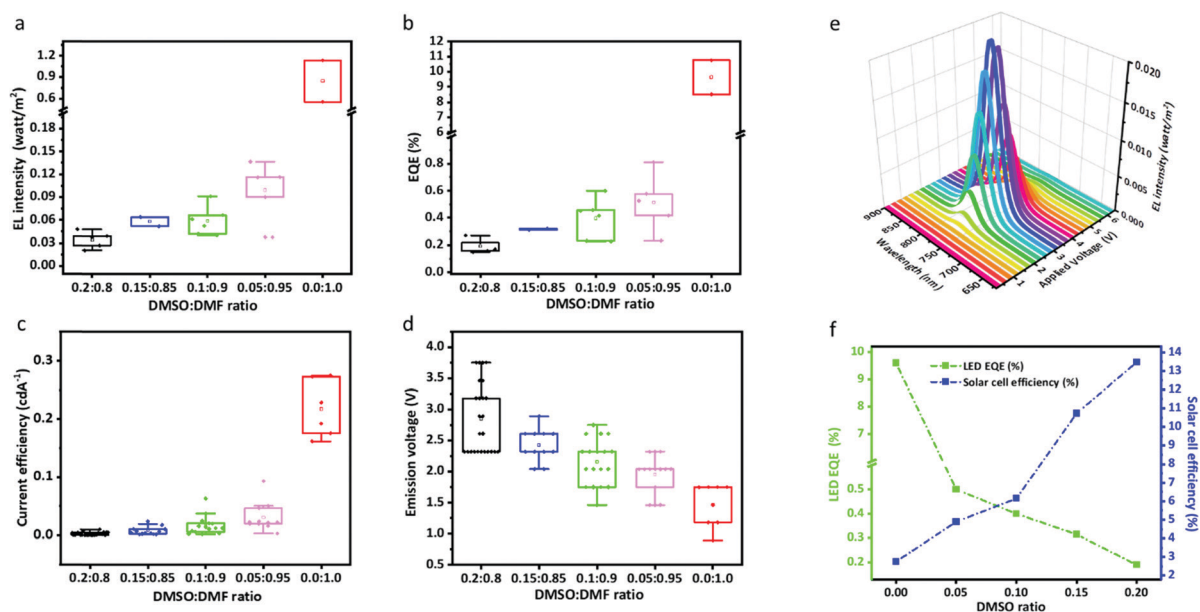


**Fig. 4** Electroluminescence (EL) measurements of LEDs for the studied DMSO : DMF ratios. (a) EL intensity measured in watt m$^{-2}$; (b) external quantum efficiency (EQE) of the LED; (c) current efficiency in cd A$^{-1}$; (d) emission voltage (V emission) is the voltage applied during the bias scan on the LED where the first EL was recorded; (e) 3D graph of EL measurement, showing the EL intensity vs. EL peak wavelength and applied voltage and (f) a comparison between the solar cell and the LED performance at different DMSO : DMF ratios.

devices without DMSO there are residues of PbI$_2$ which accumulate at the grain boundaries. The accumulation of PbI$_2$ passivate the perovskite's grains enhancing the radiative recombination,[58] therefore improving the LED performance. This further supports the increase in the EL intensity when decreasing the DMSO during the film formation.

Fig. S5b (ESI†) show that the EL peak position is shifting in a range of *ca.* 33 nm depends on the DMSO volume in the perovskite solution. In the case of only DMF the EL is red shifted compare to the other cases where DMSO is present in the perovskite solution, this shift can be attributed to emission from sub band gap levels. Evidence of multiple traps and sub band gap levels were observed in the red shifted PL (Fig. 1d) as well as the increase in the PL life time, corresponding to high trap density (Table S2, ESI†). Additional support can be seen in the peak widening as a function of the DMSO in the perovskite solution. The EL spectra of the different solvent ratios can be found in Fig. S5d (ESI†), the EL peak is widening as the DMSO is reduced with FWHM increasing from 34 nm at 0.2:0.8 DMSO:DMF ratio to 44 nm for only DMF. As discussed previously the perovskite film synthesized only by DMF show low crystallinity, pinholes and low uniformity which support the possibility of defects in the film leading to the formation of the sub band gap levels, which were found favorable of the LED performance.

Fig. 4d shows the emission voltage (V emission), correspond to the applied voltage at the time the first EL emission was recorded. As the amount of DMSO in the perovskite solution increase, the applied voltage required for the radiative recombination to occur (*i.e.* V emission) is increasing. The trend of the V emission also indicates that the perovskite layer fabricated with no DMSO, is more suitable to be used in the LED structure (due to the low V emission). The influence of the solvent ratio on the device functionality as a solar cell and as an LED can be seen in Fig. 4f. Clearly the changes to the perovskite layer with the addition of DMSO were important to achieve a better PV performance of the solar cell (with maximum PCE of 14.4%), yet when the same device was later measured as an LED it showed lower EQE and EL than devices fabricated with only DMF (EQE of 10.8%), which on the other hand didn't function well as solar cell.

The performance and characteristics of the best LED device with only DMF can be found in Fig. 5. Fig. 5a shows high current density before the device is turned on (V emission), indicating on leakage current as was also observed by low CE values (Fig. 4c). A decrease in the current density is observed at V emission due to radiative charge recombination which reduce the leakage current. Following that the current density and the EL intensity are rapidly increasing starting from 1.5 V together with strong emission by the LED. Similar trends can be observed in the Current density–Voltage–EL intensity characteristics of all DMSO:DMF ratios (Fig. S7a–d, ESI†). The LED performance is presented by the EQE–current density curve in Fig. 5b, reaching 10.8% EQE at current density of 1023.3 mA cm$^{-2}$.
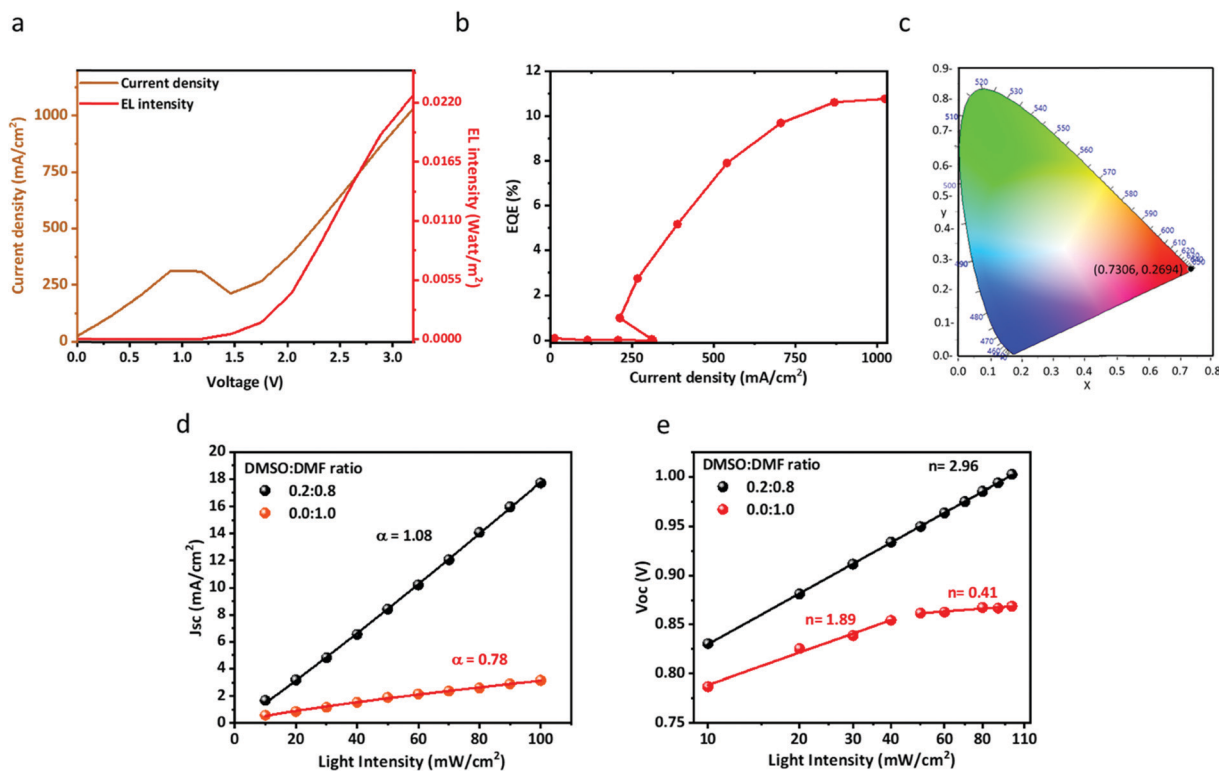


**Fig. 5** Performance and characteristics of LED with 0.0 : 1.0 DMSO : DMF solvent ratio. (a) Current density–voltage–EL intensity characteristics. (b) EQE–current density curve and (c) CIE chromaticity coordinates. The current density and the open circuit voltage at different light intensity for 0.0 : 0.1 and 0.2 : 0.8 DMSO : DMF ratios. (d) The dependence of short circuit current density ($J_{sc}$) and (e) open circuit voltage ($V_{oc}$) on light intensity.

The EQE–current density curves of all DMSO : DMF ratios can be found in Fig. S8a–d (ESI†). The Commission Internationale de l'Eclairage (CIE) color coordinates of (0.7306, 0.2694) were measured for the Near-IR emission as can be seen in Fig. 5c.

Fig. 5 presents current density and open circuit voltage measurements at different light intensities for the two limit cases of DMSO : DMF ratios. The devices were measured using under different light intensities, starting from 10 mW cm$^{-2}$ (0.1 sun) and increasing to 100 mW cm$^{-2}$ (1 sun). $JV$ curves of the devices performance under the different light intensity can be found in Fig. S9 (ESI†). The $J_{sc}$ as a function of illumination intensity is shown in Fig. 5d, the dependence is described by $J_{sc} \propto I^{\alpha}$. In the case of 0.2 : 0.8 solvent ratio $\alpha$ is 1.08, indicating on charge transfer of excited electrons to the selective contacts, which agree well with the improvement in the solar cell performance (Fig. 3). For 0.0 : 1.0 solvent ratio a lower value of $\alpha$ = 0.78 was observed indicating on the formation of space charge effects leading to charge recombination inside the layer,[59] correspond to the improvement in the EL parameters at lower DMSO ratio as can be seen in Fig. 4. Fig. 5e shows the dependence of the $V_{oc}$ as a function of the light intensity where the ideality factor, $n$ can be calculated. At 0.2 : 0.8 ratio the ideality factor ($n$) was 2.96, which indicates that the dominant mechanism is SRH with multiple trapping.[60,61] However, for 0.0 : 1.0 solvent ratio two different ideality factors can be observed. In the case of low light intensity the ideality factor was 1.89 which suggest on SRH recombination, while at high light intensity a low ideality factor of $n$ = 0.41 was obtained, suggesting that the dominant mechanism is band to band recombination. The two regions describe a two-step recombination mechanism, starting from trap filling at low light intensity, leading to non-radiative SRH recombination, followed by radiative band to band recombination. This agree well with the improved light emission, due to radiative recombination of devices without DMSO (Fig. 4a), and overall higher EQE for the LEDs (Fig. 4b).

## Conclusions

In this work we studied the effect of the solvents on the device functionality. We demonstrate that the formation of the perovskite can influence the device functionality, while keeping the same device architecture. It was found that the solvents ratio, DMSO/DMF has a major effect on the device performance as a solar cell and as an LED. The addition of DMSO to the perovskite solution is beneficial for the PV performance while only DMF is favorable for the LED performance. The solar cell requires a uniform highly crystalline perovskite film with lower amount of PbI$_2$ residues. While the LED requires more defects, higher amount of PbI$_2$ residues and is less sensitive to film uniformity. Since a solar cell and LED have an opposite mechanism the perovskite layer has a different role in these devices. Therefore, the formation conditions of the perovskite layer, the solvents ratio in the precursor's solution, are playing a significant role in the performance of these devices. As a result we were able to demonstrate PCE of 14.4% and EQE of

10.8% for the same device architecture where the perovskite is the active layer.

## Experimental section

### Preparation of perovskite solutions

Perovskite solutions were prepared in a nitrogen-filled glovebox by dissolving PbI$_2$ (Aldrich 99%), PbBr$_2$ (Aldrich $\geq$ 98%), FAI (GreatCell 99.99%) and CsI (Aldrich 99.999%) in a different solvent ratio of dimethylformamide (DMF, Aldrich anhydrous 99.8%) and dimethyl sulfoxide (DMSO, Aldrich 99.7% extra dry) at 1.25 M concentration based on the chemical formula (FA$_{0.8}$Cs$_{0.2}$)Pb(I$_{0.87}$Br$_{0.13}$)$_3$. The perovskite solutions were heated at 65 °C overnight.

### Device fabrication

Indium tin oxide (ITO) conductive glass (15 $\Omega$, Automatic Research) substrates were cleaned by four treatments of sonication bath, first in Hellmanex (2%) then deionized water, acetone and ethanol. [2-(3,6-Dimethoxy-9H-carbazol-9-yl)ethyl]phosphonic acid (MeO–2PACz) solution of 1 mg mL$^{-1}$ in Ethanol (Aldrich 99.5% Extra dry absolute) was spin coated inside a nitrogen-filled glovebox for 30 seconds at 5000 rpm on the clean substrates immediately after 15 minutes of oxygen plasma treatment, then annealed at 100 °C for 10 minutes, DMSO washing of solution excess was performed at 6000 rpm for 35 seconds, then annealed at 100 °C for 5 minutes. The perovskite was spin coated at 1000 rpm for 5 s and 5000 rpm for 50 s with chlorobenzene (Aldrich anhydrous 99.8%) anti-solvent treatment during the second spin coating step, followed by one hour annealing process. [6,6]-Phenyl-C61-butyric acid methyl ester (PCBM) (>99% Ossila) solution of 20 mg mL$^{-1}$ in chlorobenzene was deposited by dynamic spin coating at 2000 rpm for 35 seconds and annealed at 100 °C for 10 minutes. 2,9-Dimethyl-4,7-diphenyl-1,10-phenanthroline (BCP) (>99.5% Ossila) solution of 1 mg mL$^{-1}$ in isopropanol (Aldrich anhydrous 99.5%) was deposited by dynamic spin coating at 6000 rpm for 35 seconds and annealed at 70 °C for 5 minutes. 100 nm of Ag metal contact were thermally evaporated in approximately 10$^{-7}$ torr vacuum.

Scanning Electron Microscopy (SEM) cross section measurement were performed with Magellan Extra High-Resolution SEM using a FEI (field emission instruments), The Netherlands. The measurement conditions were 5 kV. Ultra High Resolution SEM measurements were performed using Sirion UHR SEM of FEI (Field Emission Instruments), The Netherlands. The measurement conditions were 10 kV.

Absorbance measurements were performed using a Jasco V-670 UV-Vis-NIR spectrophotometer.

Photoluminescence (PL) and PL life time measurements were performed for perovskite films on microscope glass, using Horiba Fluoromax-4 spectrofluorometer. The device operates with 150 W CW Ozone-free xenon arc lamp. Excitation grating of 1200 groove mm$^{-1}$ blazed at 330 nm. Emission grating of 1200 groove mm$^{-1}$ blazed at 500 nm and Photomultiplier

detector. PL life time was measured at 750 nm using a 730 nm nanoLED excitation.

Hall effect measurements were performed using Lake Shore ac/dc Hall Effect system 8404 model. A magnetic field of 1.72 T, and a current of 10 nA were used in the measurement. The samples were illuminated by 0.25 sun of white LED source. Each measurement was conducted 10 times, the average results and the standard deviations were used to the calculation of the final values, Hall effect was measured with high resistivity aperture.

X-ray diffraction (XRD) measurements were performed on a D8 Advance diffractometer (Bruker AXS, Karlsruhe, Germany) with a secondary graphite monochromator, 2° Soller slits and a 0.2 mm receiving slit. XRD patterns ranging from 2° to 75° $2\theta$ were recorded at room temperature using CuKα radiation (l = 1.5418 Å) with the following measurement conditions: a tube voltage of 40 kV, a tube current of 40 mA, a step-scan mode with a step size of 0.02° $2\theta$, and a counting time of 1 s per step.

Photovoltaic measurements were performed on a New Port system, composed of an Oriel $I–V$ test station using an Oriel Sol3A simulator. The solar simulator is class AAA for spectral performance, uniformity of irradiance, and temporal stability. The solar simulator is equipped with a 450 W xenon lamp. The output power is adjusted to match AM1.5 global sunlight (100 mW cm$^2$). The spectral match classifications are IEC60904-9 2007, JIC C 8912, and ASTM E927-05. $I–V$ curves were obtained by applying an external bias to the cell and measuring the generated photocurrent with a Keithley model 2400 digital source meter.

Electroluminescence (EL) measurements are a combination of two simultaneous measurements, emission measurements and current–voltage ($I–V$) measurements. $I–V$ curves measurements were performed using Keithley model 2400 digital source meter. EL measurements are performed using F1000-VISNIR optic fiber with cosine receptor, StellarNet BLACK-Comet Spectrometer with CRX-100 partially depleted absorber photodetector.

## Conflicts of interest

There are no conflicts to declare.

## Acknowledgements

## References

1 A. Kojima, K. Teshima, Y. Shirai and T. Miyasaka, Organometal Halide Perovskites as Visible-Light Sensitizers for Photovoltaic Cells, *J. Am. Chem. Soc.*, 2009, **131**(17), 6050–6051.

2 S. D. Stranks, G. E. Eperon, G. Grancini, C. Menelaou, M. J. P. Alcocer, T. Leijtens, L. M. Herz, A. Petrozza and H. J. Snaith, Electron-Hole Diffusion Lengths Exceeding 1 Micrometer in an Organometal Trihalide Perovskite Absorber, *Science*, 2013, **342**(6156), 341–344.

3 J. Burschka, N. Pellet, S. J. Moon, R. Humphry-Baker, P. Gao, M. K. Nazeeruddin and M. Grätzel, Sequential Deposition as a Route to High-Performance Perovskite-Sensitized Solar Cells, *Nature*, 2013, **499**(7458), 316–319.

4 Z. K. Tan, R. S. Moghaddam, M. L. Lai, P. Docampo, R. Higler, F. Deschler, M. Price, A. Sadhanala, L. M. Pazos, D. Credgington, F. Hanusch, T. Bein, H. J. Snaith and R. H. Friend, Bright Light-Emitting Diodes Based on Organometal Halide Perovskite, *Nat. Nanotechnol.*, 2014, **9**(9), 687–692.

5 B. R. Sutherland and E. H. Sargent, Perovskite Photonic Sources, *Nat. Photonics*, 2016, 295–302.

6 J. H. Noh, S. H. Im, J. H. Heo, T. N. Mandal and S. Il Seok, Chemical Management for Colorful, Efficient, and Stable Inorganic-Organic Hybrid Nanostructured Solar Cells, *Nano Lett.*, 2013, **13**(4), 1764–1769.

7 J. P. Correa-Baena, A. Abate, M. Saliba, W. Tress, T. Jesper Jacobsson, M. Grätzel and A. Hagfeldt, The Rapid Evolution of Highly Efficient Perovskite Solar Cells, *Energy Environ. Sci.*, 2017, **10**(3), 710–727.

8 G. Xing, N. Mathews, S. Sun, S. S. Lim, Y. M. Lam, M. Grätzel, S. Mhaisalkar and T. C. Sum, Long-Range Balanced Electron-and Hole-Transport Lengths in Organic-Inorganic CH3NH3PbI3, *Science*, 2013, **342**(6156), 344–347.

9 S. D. Stranks, R. L. Z. Hoye, D. Di, R. H. Friend and F. Deschler, The Physics of Light Emission in Halide Perovskite Devices, *Adv. Mater.*, 2019, 1803336.

10 S. Adjokatse, H. H. Fang and M. A. Loi, Broadly Tunable Metal Halide Perovskites for Solid-State Light-Emission Applications, *Mater. Today*, 2017, 413–424.

11 K. Lin, J. Xing, L. N. Quan, F. P. G. de Arquer, X. Gong, J. Lu, L. Xie, W. Zhao, D. Zhang, C. Yan, W. Li, X. Liu, Y. Lu, J. Kirman, E. H. Sargent, Q. Xiong and Z. Wei, Perovskite Light-Emitting Diodes with External Quantum Efficiency Exceeding 20 per Cent, *Nature*, 2018, **562**(7726), 245–248.

12 D. Ma, K. Lin, Y. Dong, H. Choubisa, A. H. Proppe, D. Wu, Y. K. Wang, B. Chen, P. Li, J. Z. Fan, F. Yuan, A. Johnston, Y. Liu, Y. Kang, Z. H. Lu, Z. Wei and E. H. Sargent, Distribution Control Enables Efficient Reduced-Dimensional Perovskite LEDs, *Nature*, 2021, **599**(7886), 594–598.

13 W. Xu, Q. Hu, S. Bai, C. Bao, Y. Miao, Z. Yuan, T. Borzda, A. J. Barker, E. Tyukalova, Z. Hu, M. Kawecki, H. Wang, Z. Yan, X. Liu, X. Shi, K. Uvdal, M. Fahlman, W. Zhang, M. Duchamp, J. M. Liu, A. Petrozza, J. Wang, L. M. Liu, W. Huang and F. Gao, Rational Molecular Passivation for High-Performance Perovskite Light-Emitting Diodes, *Nat. Photonics*, 2019, **13**(6), 418–424.

14 P. Vashishtha, S. Bishnoi, C. H. Angus Li, M. Jagadeeswararao, T. J. N. Hooper, N. Lohia, S. B. Shivarudraiah, M. S. Ansari, S. N. Sharma and J. E. Halpert, Recent Advancements in Near-Infrared Perovskite Light-Emitting Diodes, *ACS Appl. Electron. Mater.*, 2020, **2**(11), 3470–3490.

15  D. P. McMeekin, G. Sadoughi, W. Rehman, G. E. Eperon, M. Saliba, M. T. Hörantner, A. Haghighirad, N. Sakai, L. Korte, B. Rech, M. B. Johnston, L. M. Herz and H. J. Snaith, A Mixed-Cation Lead Mixed-Halide Perovskite Absorber for Tandem Solar Cells, *Science*, 2016, **351**(6269), 151–155.

16  S. Prathapani, P. Bhargava and S. Mallick, Electronic Band Structure and Carrier Concentration of Formamidinium-Cesium Mixed Cation Lead Mixed Halide Hybrid Perovskites, *Appl. Phys. Lett.*, 2018, **112**(9), 092104.

17  L. Li, Y. Chen, Z. Liu, Q. Chen, X. Wang and H. Zhou, The Additive Coordination Effect on Hybrids Perovskite Crystallization and High-Performance Solar Cell, *Adv. Mater.*, 2016, **28**(44), 9862–9868.

18  J. Lee and S. Baik, Enhanced Crystallinity of CH3NH3PbI3 by the Pre-Coordination of PbI2-DMSO Powders for Highly Reproducible and Efficient Planar Heterojunction Perovskite Solar Cells, *RSC Adv.*, 2018, 1005–1013.

19  J. H. Im, H. S. Kim and N. G. Park, Morphology-Photovoltaic Property Correlation in Perovskite Solar Cells: One-Step versus Two-Step Deposition of CH3NH3PbI 3, *APL Mater.*, 2014, **2**(8), 081510.

20  S. N. Manjunatha, Y. X. Chu, M. J. Jeng and L. B. Chang, The Characteristics of Perovskite Solar Cells Fabricated Using DMF and DMSO/GBL Solvents, *J. Electron. Mater.*, 2020, 6823–6828.

21  H. S. Kim, C. R. Lee, J. H. Im, K. B. Lee, T. Moehl, A. Marchioro, S. J. Moon, R. Humphry-Baker, J. H. Yum, J. E. Moser, M. Grätzel and N. G. Park, Lead Iodide Perovskite Sensitized All-Solid-State Submicron Thin Film Mesoscopic Solar Cell with Efficiency Exceeding 9%, *Sci. Rep.*, 2012, **2**(1), 1–7.

22  E. H. Anaraki, A. Kermanpur, L. Steier, K. Domanski, T. Matsui, W. Tress, M. Saliba, A. Abate, M. Grätzel, A. Hagfeldt and J. P. Correa-Baena, Highly Efficient and Stable Planar Perovskite Solar Cells by Solution-Processed Tin Oxide, *Energy Environ. Sci.*, 2016, **9**(10), 3128–3134.

23  T. Liu, K. Chen, Q. Hu, R. Zhu and Q. Gong, Inverted Perovskite Solar Cells: Progresses and Perspectives, *Adv. Energy Mater.*, 2016, **6**(17), 1600457.

24  J. You, Z. Hong, M. Y. Yang, Q. Chen, M. Cai, T. Bin Song, C. C. Chen, S. Lu, Y. Liu, H. Zhou and Y. Yang, Low-Temperature Solution-Processed Perovskite Solar Cells with High Efficiency and Flexibility, *ACS Nano*, 2014, **8**(2), 1674–1680.

25  Y. Zhou, M. Yang, W. Wu, A. L. Vasiliev, K. Zhu and N. P. Padture, Room-Temperature Crystallization of Hybrid-Perovskite Thin Films via Solvent-Solvent Extraction for High-Performance Solar Cells, *J. Mater. Chem. A*, 2015, **3**(15), 8178–8184.

26  H. B. Kim, Y. J. Yoon, J. Jeong, J. Heo, H. Jang, J. H. Seo, B. Walker and J. Y. Kim, Peroptronic Devices: Perovskite-Based Light-Emitting Solar Cells, *Energy Environ. Sci.*, 2017, **10**(9), 1950–1957.

27  D. Bi, W. Tress, M. I. Dar, P. Gao, J. Luo, C. Renevier, K. Schenk, A. Abate, F. Giordano, J. P. Correa Baena, J. D. Decoppet, S. M. Zakeeruddin, M. K. Nazeeruddin, M. Grätzel and A. Hagfeldt, Efficient Luminescent Solar Cells Based on Tailored Mixed-Cation Perovskites, *Sci. Adv.*, 2016, **2**(1), e1501170.

28  W. Tress, N. Marinova, O. Inganäs, M. K. Nazeeruddin, S. M. Zakeeruddin and M. Graetzel, Predicting the Open-Circuit Voltage of CH3NH3PbI3 Perovskite Solar Cells Using Electroluminescence and Photovoltaic Quantum Efficiency Spectra: The Role of Radiative and Non-Radiative Recombination, *Adv. Energy Mater.*, 2015, **5**(3), 1400812.

29  U. Rau, Reciprocity Relation between Photovoltaic Quantum Efficiency and Electroluminescent Emission of Solar Cells, *Phys. Rev. B: Condens. Matter Mater. Phys.*, 2007, **76**(8), 085303.

30  S. Mastroianni, F. D. Heinz, J. H. Im, W. Veurman, M. Padilla, M. C. Schubert, U. Würfel, M. Grätzel, N. G. Park and A. Hinsch, Analysing the Effect of Crystal Size and Structure in Highly Efficient CH3NH3PbI3 Perovskite Solar Cells by Spatially Resolved Photo- and Electroluminescence Imaging, *Nanoscale*, 2015, **7**(46), 19653–19662.

31  M. Rai, L. H. Wong and L. Etgar, Effect of Perovskite Thickness on Electroluminescence and Solar Cell Conversion Efficiency, *J. Phys. Chem. Lett.*, 2020, **11**(19), 8189–8194.

32  W. Li, J. Fan, J. Li, Y. Mai and L. Wang, Controllable Grain Morphology of Perovskite Absorber Film by Molecular Self-Assembly toward Efficient Solar Cell Exceeding 17%, *J. Am. Chem. Soc.*, 2015, **137**(32), 10399–10405.

33  W. S. Yang, J. H. Noh, N. J. Jeon, Y. C. Kim, S. Ryu, J. Seo and S. Il Seok, High-Performance Photovoltaic Perovskite Layers Fabricated through Intramolecular Exchange, *Science*, 2015, **348**(6240), 1234–1237.

34  J. Liu, B. Chen, Q. Wang, R. Li, B. Shi, Y. Li, F. Hou, X. Cui, P. Wang, Y. Li, Y. Zhao and X. Zhang, Self-Formed PbI2-DMSO Adduct for Highly Efficient and Stable Perovskite Solar Cells, *Appl. Phys. Lett.*, 2019, **115**(23), 233901.

35  N. Ahn, D. Y. Son, I. H. Jang, S. M. Kang, M. Choi and N. G. Park, Highly Reproducible Perovskite Solar Cells with Average Efficiency Of, *J. Am. Chem. Soc.*, 2015, 475–480.

36  F. H. Isikgor, A. S. Subbiah, M. K. Eswaran, C. T. Howells, A. Babayigit, M. De Bastiani, E. Yengel, J. Liu, F. Furlan, G. T. Harrison, S. Zhumagali, J. I. Khan, F. Laquai, T. D. Anthopoulos, I. McCulloch, U. Schwingenschlögl and S. De Wolf, Scaling-up Perovskite Solar Cells on Hydrophobic Surfaces, *Nano Energy*, 2021, **81**, 105633.

37  D. P. McMeekin, Z. Wang, W. Rehman, F. Pulvirenti, J. B. Patel, N. K. Noel, M. B. Johnston, S. R. Marder, L. M. Herz and H. J. Snaith, Crystallization Kinetics and Morphology Control of Formamidinium–Cesium Mixed-Cation Lead Mixed-Halide Perovskite via Tunability of the Colloidal Precursor Solution, *Adv. Mater.*, 2017, **29**(29), 1607039.

38  L. K. Ono, E. J. Juarez-Perez and Y. Qi, Progress on Perovskite Materials and Solar Cells with Mixed Cations and Halide Anions, *ACS Appl. Mater. Interfaces*, 2017, 30197–30246.

39  Y. Rong, Z. Tang, Y. Zhao, X. Zhong, S. Venkatesan, H. Graham, M. Patton, Y. Jing, A. M. Guloy and Y. Yao, Solvent Engineering towards Controlled Grain Growth in

Perovskite Planar Heterojunction Solar Cells, *Nanoscale*, 2015, **7**(24), 10595–10599.

40  Y. Jo, K. S. Oh, M. Kim, K. H. Kim, H. Lee, C. W. Lee and D. S. Kim, High Performance of Planar Perovskite Solar Cells Produced from PbI2(DMSO) and PbI2(NMP) Complexes by Intramolecular Exchange, *Adv. Mater. Interfaces*, 2016, **3**(10), 15007.

41  Y. H. Seo, E. C. Kim, S. P. Cho, S. S. Kim and S. I. Na, High-Performance Planar Perovskite Solar Cells: Influence of Solvent upon Performance, *App. Mater. Today*, 2017, 598–604.

42  I. Montoya De Los Santos, H. J. Cortina-Marrero, M. A. Ruíz-Sánchez, L. Hechavarría-Difur, F. J. Sánchez-Rodríguez, M. Courel and H. Hu, Optimization of CH3NH3PbI3 Perovskite Solar Cells: A Theoretical and Experimental Study, *Sol. Energy*, 2020, **199**, 198–205.

43  H. D. Kim, H. Ohkita, H. Benten and S. Ito, Photovoltaic Performance of Perovskite Solar Cells with Different Grain Sizes, *Adv. Mater.*, 2016, **28**(5), 917–922.

44  H. Cho, S. H. Jeong, M. H. Park, Y. H. Kim, C. Wolf, C. L. Lee, J. H. Heo, A. Sadhanala, N. S. Myoung, S. Yoo, S. H. Im, R. H. Friend and T. W. Lee, Overcoming the Electroluminescence Efficiency Limitations of Perovskite Light-Emitting Diodes, *Science*, 2015, **350**(6265), 1222–1225.

45  Z. Xiao, R. A. Kerner, L. Zhao, N. L. Tran, K. M. Lee, T. W. Koh, G. D. Scholes and B. P. Rand, Efficient Perovskite Light-Emitting Diodes Featuring Nanometre-Sized Crystallites, *Nat. Photonics*, 2017, **11**(2), 108–115.

46  D. H. Ma, W. J. Zhang, Z. Y. Jiang, D. Y. Song, L. Zhang and W. Yu, Enhanced Photovoltaic Performance of the Inverted Planar Perovskite Solar Cells by Using Mixed-Phase Crystalline Perovskite Film with Trace Amounts of PbI2 as an Absorption Layer, *J. Phys. Chem. C*, 2017, **121**(41), 22607–22620.

47  D. Shi, V. Adinolfi, R. Comin, M. Yuan, E. Alarousu, A. Buin, Y. Chen, S. Hoogland, A. Rothenberger, K. Katsiev, Y. Losovyj, X. Zhang, P. A. Dowben, O. F. Mohammed, E. H. Sargent and O. M. Bakr, Low Trap-State Density and Long Carrier Diffusion in Organolead Trihalide Perovskite Single Crystals, *Science*, 2015, **347**(6221), 519–522.

48  R. Li, H. Zhang, M. Zhang and M. Guo, Effect of PbI 2 Solution on Air-Preparation of Perovskite Solar Cells for Enhanced Performance, *Appl. Surf. Sci.*, 2018, **458**, 172–182.

49  F. Hao, C. C. Stoumpos, P. Guo, N. Zhou, T. J. Marks, R. P. H. Chang and M. G. Kanatzidis, Solvent-Mediated Crystallization of CH3NH3SnI3 Films for Heterojunction Depleted Perovskite Solar Cells, *J. Am. Chem. Soc.*, 2015, **137**(35), 11445–11452.

50  B. El Cohen, Y. Li, Q. Meng and L. Etgar, Dion-Jacobson Two-Dimensional Perovskite Solar Cells Based on Benzene Dimethanammonium Cation, *Nano Lett.*, 2019, **19**(4), 2588–2597.

51  A. Shpatz Dayan, X. Zhong, M. Wierzbowska, C. E. M. de Oliveira, A. Kahn and L. Etgar, The Properties, Photovoltaic Performance and Stability of Visible to near-IR All Inorganic Perovskites, *Mater. Adv.*, 2020, **1**(6), 1920–1929.

52  Y. Chen, H. T. Yi, X. Wu, R. Haroldson, Y. N. Gartstein, Y. I. Rodionov, K. S. Tikhonov, A. Zakhidov, X. Y. Zhu and V. Podzorov, Extended Carrier Lifetimes and Diffusion in Hybrid Perovskites Revealed by Hall Effect and Photoconductivity Measurements, *Nat. Commun.*, 2016, **7**(1), 1–9.

53  B. Cai, W. H. Zhang and J. Qiu, Solvent Engineering of Spin-Coating Solutions for Planar-Structured High-Efficiency Perovskite Solar Cells, *Chin. J. Catal.*, 2015, **36**(8), 1183–1190.

54  P. W. Liang, C. C. Chueh, S. T. Williams and A. K. Y. Jen, Roles of Fullerene-Based Interlayers in Enhancing the Performance of Organometal Perovskite Thin-Film Solar Cells, *Adv. Energy Mater.*, 2015, **5**(10), 1402321.

55  D. Luo, W. Yang, Z. Wang, A. Sadhanala, Q. Hu, R. Su, R. Shivanna, G. F. Trindade, J. F. Watts, Z. Xu, T. Liu, K. Chen, F. Ye, P. Wu, L. Zhao, J. Wu, Y. Tu, Y. Zhang, X. Yang, W. Zhang, R. H. Friend, Q. Gong, H. J. Snaith and R. Zhu, Enhanced Photovoltage for Inverted Planar Heterojunction Perovskite Solar Cells, *Science*, 2018, **360**(6396), 1442–1446.

56  A. Al-Ashouri, A. Magomedov, M. Roß, M. Jošt, M. Talaikis, G. Chistiakova, T. Bertram, J. A. Márquez, E. Köhnen, E. Kasparavičius, S. Levcenco, L. Gil-Escrig, C. J. Hages, R. Schlatmann, B. Rech, T. Malinauskas, T. Unold, C. A. Kaufmann, L. Korte, G. Niaura, V. Getautis and S. Albrecht, Conformal Monolayer Contacts with Lossless Interfaces for Perovskite Single Junction and Monolithic Tandem Solar Cells, *Energy Environ. Sci.*, 2019, **12**(11), 3356–3369.

57  N. G. Park, Perovskite Solar Cells: An Emerging Photovoltaic Technology, *Materials Today*, 2015, 65–72.

58  T. J. Jacobsson, J. P. Correa-Baena, E. Halvani Anaraki, B. Philippe, S. D. Stranks, M. E. F. Bouduban, W. Tress, K. Schenk, J. Teuscher, J. E. Moser, H. Rensmo and A. Hagfeldt, Unreacted PbI2 as a Double-Edged Sword for Enhancing the Performance of Perovskite Solar Cells, *J. Am. Chem. Soc.*, 2016, **138**(32), 10331–10343.

59  V. D. Mihailetchi, J. Wildeman and P. W. M. Blom, Space-Charge Limited Photocurrent, *Phys. Rev. Lett.*, 2005, **94**(12), 126602.

60  T. Singh and T. Miyasaka, Stabilizing the Efficiency Beyond 20% with a Mixed Cation Perovskite Solar Cell Fabricated in Ambient Air under Controlled Humidity, *Adv. Energy Mater.*, 2018, **8**(3), 1700677.

61  W. Tress, M. Yavari, K. Domanski, P. Yadav, B. Niesen, J. P. Correa Baena, A. Hagfeldt and M. Graetzel, Interpretation and Evolution of Open-Circuit Voltage, Recombination, Ideality Factor and Subgap Defect States during Reversible Light-Soaking and Irreversible Degradation of Perovskite Solar Cells, *Energy Environ. Sci.*, 2018, **11**(1), 151–165.